

Dry Sliding Wear Resistance of Fe-Cr-C hardfacing Deposited by Flux-Core-Double-Wire GTAW

Fernando Henrique Gruber Colaço^a , Arthur Henrique Ribeiro Souto^a, Joel Stryhalski^{**} ,
Gil Magno Portal Chagas^a , Almir Turazi^a , Alexandre Galiotto^a , Giuseppe Pintaude^b 

^aInstituto Federal de Santa Catarina (IFSC), Departamento de Engenharia Mecânica,
Rua dos Imigrantes, 445, 89254-630, Jaraguá do Sul, SC, Brasil.

^bUniversidade Tecnológica Federal do Paraná (UTFPR), Programa de Pós-Graduação em
Engenharia Mecânica (PPGEM), Rua Deputado Heitor de Alencar Furtado, 5000, 81280-340,
Curitiba, PR, Brasil.

Received: December 16, 2022; Revised: April 28, 2023; Accepted: May 25, 2023

Gas-Shielded Tungsten Arc Welding (GTAW) was modified to a Flux-Cored-Double-Wire GTAW (FCDW-GTAW); in this technique, wires of different compositions are used simultaneously to obtain different microstructures. In the modified GTAW, automatic flux-cored double-wire was used with a combination of four different wires deposited in AISI1020 steel, allowing different microstructures. Pin-on-disk wear tests described by ASTM G99 was used to evaluate the wear coefficients of four hardfacing materials combining Fe-Cr-C, Fe-Cr-C-Nb, Fe-Cr-C-Mo-Nb, and Fe-Cr-C-Mo-Ti alloys. The combination of these wires resulted in a hypoeutectic microstructure with niobium and titanium carbides, with an average hardness of 650 HV_{0.3}, and hypereutectic microstructures formed by different niobium contents, with a microhardness range from 820 to 1020 HV_{0.3}. The wear tests were performed without lubrication at room temperature, using a 6.0 mm diameter polished alumina sphere as a counter-body. The total distance covered was 1000 m with a speed of 0.1 m/s, a track radius of 6.0 cm, and an applied load of 10 N. Hardness, microstructure, wear coefficient, and wear mechanisms were compared. The results showed that wear resistance could be differentiated by the predominant wear mechanism: polishing for the hypoeutectic hardfacing and cracking for the hypereutectic ones.

Keywords: GTAW, Hardfacing, Wear-Resistance, Wear-mechanisms, Carbides.

1. Introduction

Mechanical components of heavy equipment, such as crushers and wheel loaders in the mining sector and agricultural or civil construction machinery, are usually subjected to severe wear conditions due to direct exposure of components to abrasive particles such as sand and stones. This fact can generate financial losses with stoppages in the production process for maintenance or replacement with new parts. Therefore, the reduction of costs in the manufacture of these components is significant in the industry. One of the ways to improve wear resistance is hardfacing. This procedure uses the application of a filler metal that is harder than the substrate, improving the tribological properties and extending the life time of the components¹⁻³. The deposition of coatings via electric arc shows excellent results in abrasion resistance applications⁴⁻⁶. Hard coatings deposited by GTAW (gas tungsten arc welding)⁷ and PAW (plasma arc welding)⁸ can present substrate dilutions below 30% with few defects, and the dilution can vary according to the thickness of the deposited coating, reaching around 5% dilution⁹. The dilution percentage is one of the factors that most contribute to the performance of the coating, directly influencing the percentage of alloying elements and, consequently, the hardness and wear resistance⁶.

Among various electric arc processes available, the deposition technique through the GTAW (gas tungsten arc welding) can be advantageous because parameters like wire material, wire feed speed, and welding energy are directly correlated with deposition rate, base material heating, and, consequently, dilution rate.

The composition of the filler material for hardfacing purposes generally contains a high content of hard phase forming elements, mainly carbides¹⁰. In wear conditions, the ideal is that the microstructure presents moderate matrix hardness and resistance to the support of the second hard phase¹¹. However, it is interesting that the microstructure has an excellent volumetric fraction and second phase size, so the mean free path between the carbides does not allow the abrasive to penetrate more into the matrix, removing more material^{11,12}.

It is possible to obtain hard coatings with various compositions, which enables the optimization of wear-resistant surfaces containing low dilution rates. The hypereutectic Fe-Cr-C alloys for hardfacing require low dilution rates to ensure the specified chemical composition and thus the precipitation of primary M₇C₃ carbides, which affect the abrasive wear resistance of the hardfacing¹³. According to Bewley¹⁴, the lower dilution provided by techniques such as arc welding is because, in this process, the energy of the arc acts on the weld pool, isolating the substrate from direct contact with the arc.

*e-mail: joel@ifsc.edu.br

Because dilution is critical in determining wear performance, the development of deposition welding processes with reduced thermal impact and hence reduced base material dilution is the objective of this study.

The present investigation applies Flux-Cored-Double-Wire (FCDW-GTAW) technique to manufacture hardfacings. It aims to describe the wear performance under the pin-on-disk test of hardfacings based on chromium carbides and to determine the effects of adding various carbide-forming elements (Ti, Nb, and Mo). It was done by manipulating the microstructure of hard coatings by applying the double wire deposition technique (FCDW-GTAW)¹⁵⁻¹⁷, and wear performance was evaluated in a pin-on-disk wear test.

In terms of the practical application of these coatings, it is commonly used, characterizing carrying out tests such as abrasion, erosion, and wear tests. In this work, a pin-on-disk configuration for investigating the wear mechanism or behavior of solid materials was scrutinized since the results of such configurations can differ from published data¹⁸. The ASTM G99¹⁹ standard was applied to avoid variations due to test speeds, track radius, and applied load.

In addition, the pin-on-disk wear test is a commonly used method for evaluating the wear resistance of materials. The advantage of a wear test, when compared to indentation or scratch testing, is that it can measure the lifetime of a particular coating-substrate system. In many coatings applications, the resistance to wear can be more important than the load required to damage the material permanently²⁰. Finally, the pin-on-disk wear test provides a reliable and widely used scientific community for evaluating the performance of hardfacing materials, making it an essential tool for researchers and engineers in materials science.

Results were observed in the base metal's low dilution and obtaining distinct microstructures by manipulating the dilution and microstructure independently. The wear coefficients and the microstructure characteristics were compared to the wear mechanisms, making it possible to determine how the wear resistance can be differentiated by the hardness of the second hard phase and by the resistance of the metallic matrix to carbide support.

2. Experimental Procedure

2.1. Equipment and materials

Four hardfacings were produced on AISI 1020 steel substrate of size 6 x 150 x 200 mm by FCDW-GTAW process, combining two different flux core wires with 1.6mm diameter and composition shown in Table 1.

The identification used for the individual wires (Ti, HCr, Nb, and NbMo) and the generated hardfacings (Ti-NbMo, HCr-Nb, HCr-NbMo, and Nb-NbMo) is based on the element with the highest concentration and the main carbide-forming alloying elements. The combination of the four wires was chosen to obtain coatings with a higher concentration of the chemical element prevalent in each wire.

The use of AISI 1020 steel in this work is justified due to several factors:

1. AISI 1020 is a widely available, cost-effective, low-carbon steel commonly used in various industrial applications.
2. AISI1020 steel exhibits good machinability and weldability, which makes it easy to work with and process. It is crucial for researchers who need to fabricate test specimens or components with specific geometries or properties for their experiments.
3. AISI1020 steel has been extensively studied and characterized, with a significant substrate in the literature on its mechanical, physical, and chemical properties. It makes it a well-understood material widely used as a reference or benchmark material for comparative studies.
4. AISI1020 steel is a commonly used material in many engineering and industrial applications, making the results obtained from scientific studies using this material highly relevant and applicable to real-world situations.

Overall, using AISI1020 steel in scientific work is justified due to its availability, cost-effectiveness, ease of processing, extensive characterization, and relevance to real-world applications.

The welding source used to manufacture the beads was Sumig; Lion 300. The compatibility of a metal hardfacing flux-cored wire was tested using a five-factor, five-level central composite design (CCD) matrix¹⁶ varying welding current, welding speed, nozzle standoff distance, travel angle, and wire feed pulse frequency. The combination of low dilution and good surface quality of the beads was used as a criterion for selecting parameters. The electrical parameters for manufacturing the single-layer coatings defined from the CCD design matrix were an average welding pulsed current of 230 A ($\pm 25\%$) and a welding voltage of 20 V. The torch was fixed on the welding manipulator at 15 degrees and a speed of $0.15 \text{ m} \cdot \text{min}^{-1}$ at a distance of 12 mm. The tungsten electrode (W - 1.5%La) with a diameter of 3.2 mm and a tip of 40° was employed. An argon flow rate of $14 \text{ L} \cdot \text{min}^{-1}$ and a number 8 ceramic nozzle were used to protect the weld pool.

Table 1. Chemical composition of the wire materials used.

Wire name	Wire chemical composition (Weight, %)										
	C	Si	Mn	Cr	Mo	V	W	Nb	Ti	B	Fe
Ti	2.00	0.40	1.00	6.5	1.10	–	–	–	6.00	–	Bal.
HCr	3.34	0.82	0.314	27.00	0.026	–	0.007	–	0.010	0.311	Bal.
Nb	3.41	1.05	0.228	17.88	–	–	–	3.06	–	–	Bal.
NbMo	4.56	0.57	0.25	19.00	6.11	0.67	1.53	5.50	–	–	Bal.

The wires were fed into the weld pool at a speed of $4.7 \text{ m} \cdot \text{min}^{-1}$. The inclination of the wires in the feeding direction was 20° . The substrate was heated to a temperature of 150°C for the deposition of the coatings. Figure 1 shows (a) GTAW system with dual feed configuration, (b) weld region; and (c) wire positioning, where H is the standoff distance (10 mm), and D is the torch angle (15°).

2.2. Samples characterization

The hardness of hardfacing was determined using Vickers hardness testing with a 300 g load ($\text{HV}_{0.3}$) and a dwell time of 10 seconds. Each hardness value was the average result of at least 50 measurements.

The microstructure and volume fraction of carbides was obtained in 24 images (magnification 100x) and analyzed in Olympus BX-51 optical microscopy (OM). The specimen was polished and etched with the Marble reagent of 4 g $\text{CuSO}_4 + 20 \text{ ml HCl} + 20 \text{ ml H}_2\text{O}$ to reveal particles and matrix.

The stoichiometry and morphology of hardfacings formed on AISI 1020 steel were analyzed by X-ray diffraction (XRD) Shimadzu model XRD-7000, with $\text{Cu K}\alpha$ radiation at a scan rate of 2° min^{-1} within the angle range of $20\text{--}130^\circ$. Scanning Electron Microscopy (SEM) Carl Zeiss, model EVO MA 15, and Energy Dispersion X-Ray Spectroscopy (EDS) Oxford X-Max were used to analyze the microstructure, wear mechanisms, and distribution of elements.

2.3. Wear tests

Pin-on-disk tests were carried out on each specimen at room temperature and without lubrication. Four replicas were performed on each condition. The ASTM G99 standard¹⁹ described the test, and a schematic diagram of the system is shown in Figure 2a.

The tests used 30 mm diameter samples and were performed with a sliding speed of 0.1 m/s, and the total distance was 1000 m and 5 mm track radius. The counter-body was a polished alumina (Al_2O_3) ball with a 6 mm diameter and a load of 10 N. Figure 2b illustrates a worn area mapping acquired through interferometer Taly Surf CCI Lite Non-contact 3D in order to calculate the volume of removed material. The volume of material removed (V) was calculated by multiplication of the average wear track area by the track length $2\pi R$, where R is the wear track radius. The average cross-sectional area was determined in 4 points of each sample, as shown in Figure 2b.

The wear coefficient was calculated using the Archard model (Equation 1), where V is the volume loss, H is hardness, and N is a normal force due to applied load and sliding distance (S)²².

$$k = V \cdot H (N \cdot S)^{-1} \quad (1)$$

3. Results and Discussion

3.1. Microstructure

Figure 3 shows the results of the phases of the four hardfacings performed by DRX. The diffraction peaks show that the microstructure of the hypoeutectic coating Ti-NbMo presented the microconstituents of austenite (peak 2 in XRD) and primary carbides of titanium (TiC) (peak 5) and niobium (NbC) (peak 4) dispersed in a eutectic matrix of austenite and chromium carbides (M_7C_3) (peak 6). The hypereutectic microstructures presented diffraction peaks related to the constituent's chromium carbides (M_7C_3) (peak 6), niobium carbides (MC type) (peak 4), cementite (peak 3), austenite (peak 2), and martensite (peak 1) in the Nb-NbMo, HCr-Nb, HCr-NbMo hardfacings.

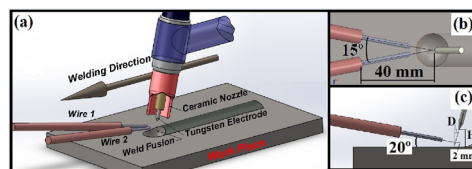


Figure 1. (a) GTAW system with double-feed configuration; (b) Weld pool region; and (c) Positioning of wires, where H is the standoff distance (10 mm) and D is the torch angle (15°)¹⁷.

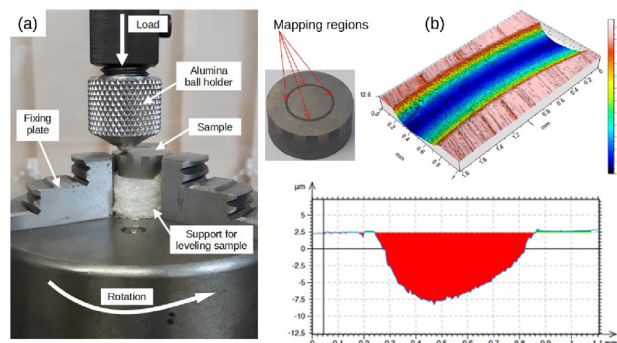


Figure 2. (a) Illustration of the pin-on-disk sliding test, (b) illustration of wear track area and points used in interferometer measurements to calculate VMR, adapted from²¹.

The reference letters used to identify these phases were: austenite (γ -Fe) (JCPDS code: 96-901-4477), martensite (α -Fe) (JCPDS code: 00-006-0696), iron carbides (Fe_3C) (JCPDS code: 01-072-1110), titanium carbides (TiC) (JCPDS code: 01-073-0472) and niobium carbides (NbC) (JCPDS code: 01-074-1222) and carbides M_7C_3 (JCPDS code: 078-1502).

Only the Ti-NbMo hardfacing combination showed a hypoeutectic microstructure, consisting of the primary solidification of titanium and niobium carbides (MC type) dispersed in a eutectic matrix. These carbides are typically classified as high-entropy carbides^{23,24}. A hypothesis for the alloy to become hypoeutectic is that the titanium and niobium carbides solidify before the matrix, which changes the stoichiometry of the carbide phase and strengthens it

by including these new atoms into the TiC constituent, or even more, by promoting the formation of primary carbides (the first phase solidifying before austenite dendrites) which at the end of the solidification process can remain within the austenitic matrix²⁵.

The other combinations were hypereutectic with several primary chromium carbides M_7C_3 and niobium carbides NbC dispersed in a eutectic matrix formed by austenite and carbides M_7C_3 .

The microstructure of the hypoeutectic hardfacing Ti-NbMo (a) and hypereutectic hardfacings HCr-Nb (b), HCr-NbMo (c), Nb-NbMo (d) are shown in Figure 4. Fe_3C in low quantity in hypoeutectic Ti-MoNb can reduce the adhesive wear and friction coefficient, consequently can reduce the wear performance as related in similar studies^{21,26,27}.

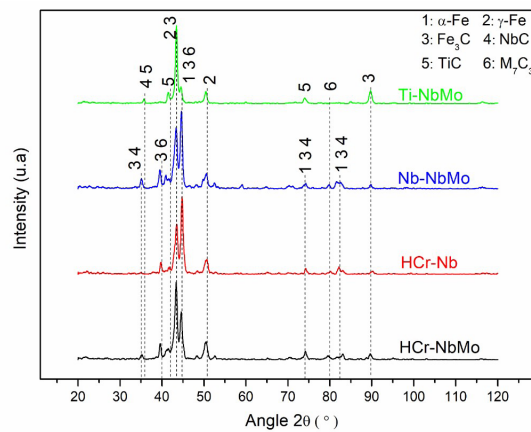


Figure 3. X-ray diffraction pattern of hardfacings.

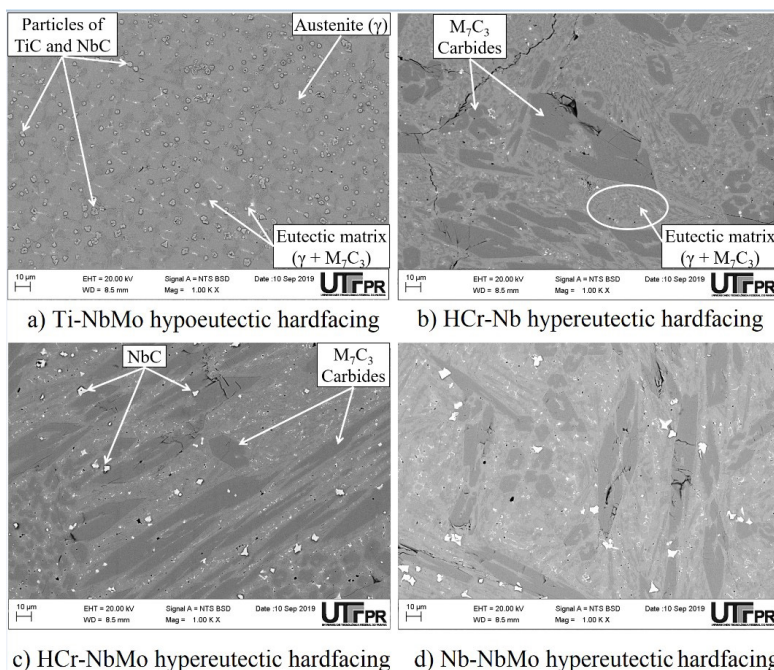


Figure 4. Microstructure of hypoeutectic hardfacing (a) Ti-NbMo and hypereutectic hardfacings (b) HCr-Nb, (c) HCr-NbMo, and (d) Nb-NbMo.

3.2. Wear behavior

Topographic measurements quantified the worn tracks produced during pin-on-disk tests to evaluate the tribological performance. As shown in Figure 5, the cross-sectional area of the wear track reflected the alumina counter-body geometry. The average track radius was 5.2 mm, and the volume of removed material for each hardfacing sample was calculated with an average of 4 points for each sample. The dimensionless Archard wear coefficients were obtained according to the Archard²², Huq and Celis²⁸ model and are shown in Table 2.

The microhardness of hypoeutectic and hypereutectic microstructures is shown in Table 2. Combining Ti wire with NbMo forms the hypoeutectic Ti-NbMo hardfacing. A lack of carbon can explain a hypoeutectic matrix with an approximate hardness of $651 \pm 148 \text{ HV}_{0.3}$. Despite the presence of titanium and niobium carbides MC-type, which have high hardness, the hypoeutectic matrix is soft, and their presence may be responsible for reducing the hardness of this coating^{29,30}. The other coatings are hypereutectic and show a higher hardness, ranging from 820 to $1020 \text{ HV}_{0.3}$, and wear coefficient, as shown in Table 2.

The softest coatings (Ti-NbMo and HCr-Nb) resulted in the highest volumes of material removed.

The coefficient of variation is relatively high for wear volumes, reaching 30% for HCr-NbMo coating. When the micro-cracking mechanism is predominant, the variation in wear volumes is usually high, for example, as demonstrated by Bozzi and de Mello³¹ for HVOF coatings. In their study, it was difficult to define the end of the running-in period because the high coefficients of variation did not reach values considered reasonable compared to systems where other wear mechanisms were predominant.

The determined values and standard deviations in dimensionless Archard wear coefficient (Figure 6) show similar values for hypereutectic hardfacings and the lowest value obtained for the Ti-NbMo coating.

Different values of the wear coefficient can represent a specific change in the wear mechanism³². In this fashion, one could expect similar mechanisms for all hypereutectic coatings and a different one for the hypoeutectic. Figure 7 illustrates the worn tracks for each studied hardfacing, revealed using SEM.

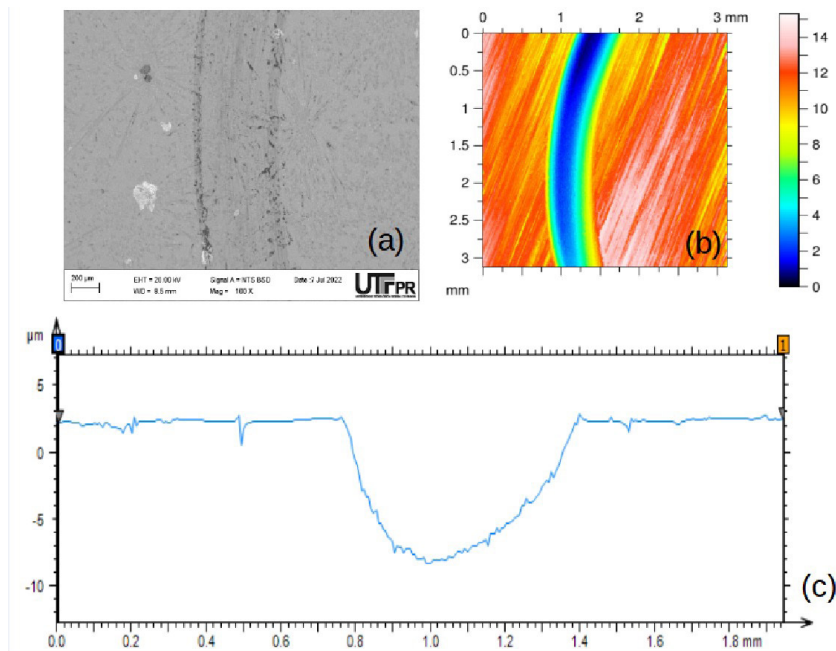


Figure 5. Topographic analysis of the worn section after the pin-on-disk tribological test, (a) SEM wear track, (b) wear track interferometer image and, (c) profile curve MountainsMap® surface analysis software.

Table 2. Hardness, volume fraction of carbides, volume of removed material, and wear coefficient of the hardfacings Ti-NbMo (a); HCr-Nb (b); HCr-NbMo (c); Nb-NbMo (d).

	Hardness [HV _{0.3}]	Volume Fraction of Carbides [%]	Volume of removed Material [mm ³]	Wear coefficient ($\cdot 10^{-5}$) [dimensionless]
(a) Ti-NbMo	651 ± 148	12 ± 3	0.11 ± 0.02	$7 + 1$
(b) HCr-Nb	826 ± 78	14 ± 3	0.11 ± 0.02	$9 + 2$
(c) HCr-NbMo	893 ± 118	19 ± 4	0.10 ± 0.03	$9 + 2$
(d) Nb-NbMo	913 ± 103	25 ± 4	0.10 ± 0.02	$9 + 1$

Figure 7a shows very thin scratches along with the image. They are related to the presence of carbides, harder than the asperities of alumina balls. The possibility of scratching the surface created an event similar to metallographic preparation, the comet tails, indicated in this Figure. The metallic matrix was severely deformed, and more details of this mechanism will be checked in Figure 8. One can observe fractured regions in Figures 7b, 7c, and 7d. In all cases, these regions are associated with M_7C_3 carbides, which occupy a much larger area than the others. Another common feature is the presence of gray regions characterized by oxides. This oxidation is proof of heating during the sliding process, and the portion created by the carbides pull-out could expose new regions unevenly concerning the original regions. These areas were oxidized preferentially, but as the sliding proceeded, cracks were also observed within the oxides, making this micro-mechanism predominant for all hardfacings, leading to similar wear coefficients.

The extension of plastic deformation can be checked using H^3/E^2 relation. This index indicates the possibility of a circular contact surpassing the yielding point. Using the smaller value determined for hypoeutectic hardfacing and an elastic modulus of 200 GPa, we determined a value of 0.003. On the other hand, considering the data published by Jokari-Sheshdeh et al.³³ for different $(Cr, Fe)_7C_3$ ternary carbides for their tougher cast iron, one can calculate an index of 0.121, i.e., two orders of magnitude higher than the value found for our softest case. This difference is an excellent indicator of the limited possibility of deforming in an extensive way the hypereutectic samples. Additionally, we can affirm that the massive presence of carbides for the sliding conditions selected herein was not beneficial to the performance of hardfacings, an opposite result as described elsewhere under microabrasion conditions¹⁷. The wear variables, especially the contact pressure and sliding velocity, were aggressive enough to promote the observed wear mechanisms.

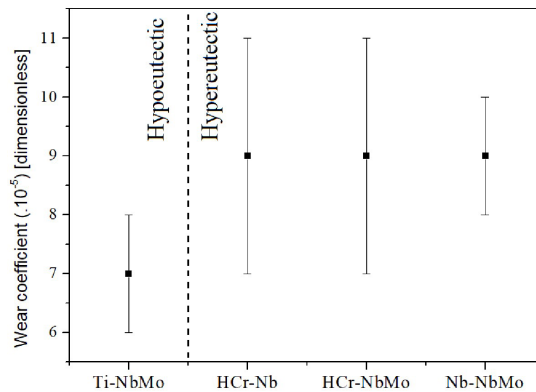


Figure 6. Dimensionless wear coefficient for each hardfacing.

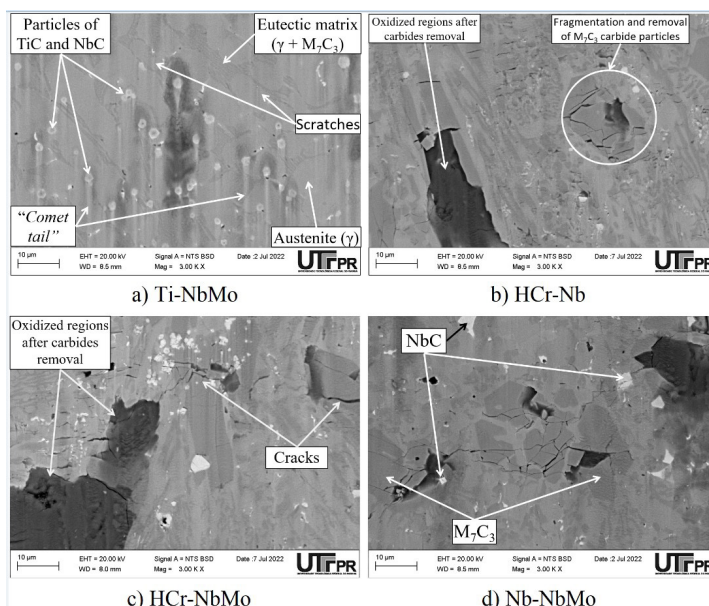


Figure 7. SEM images showing wear mechanisms: (a). Ti-NbMo and hypereutectic hardfacings (b) HCr-Nb, (c) HCr-NbMo, and (d) Nb-NbMo.

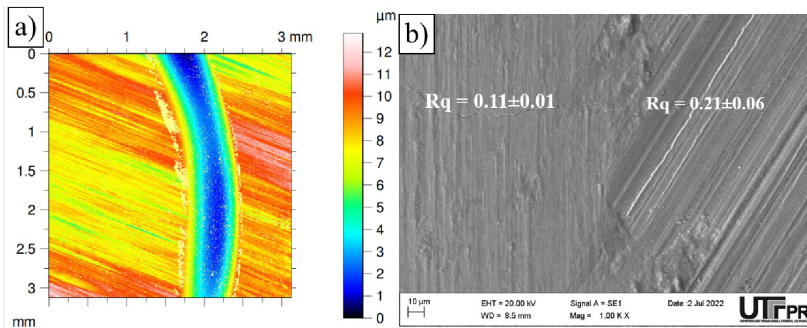


Figure 8. Topographic images of Ti-NbMo coating after pin-on-disc test.

The plastic deformation in hypoeutectic hardfacing can be seen in Figure 8. We can note a significant change in surface texture inside the worn track: the original surface before sliding wear is anisotropic, while after the wear process, it became isotropic. The reduction in root mean square of surface roughness, determined transversal to machined marks, was significant: 47.6%. This reduction is proof of the polishing mechanism described in Figure 7a for this hardfacing, besides the extensive plastic deformation.

4. Conclusions

Fe-Cr-C-based hardfacings deposited on AISI 1020 steel using the FCDW-GTAW process were investigated on a pin-on-disk wear test. The following conclusions can be drawn:

- Two kinds of microstructures were obtained: hypoeutectic ones with small MC carbides and hypereutectic ones with massive M_7C_3 carbides;
- The wear coefficient was smaller for the hypoeutectic hardfacing, which was plastically deformed and polished by alumina ball asperities;
- The predominant mechanism observed for hypereutectic hardfacings was micro-cracking of M_7C_3 carbides. The pulled-out regions of carbides suffered intense oxidation, which was also fractured as wear process continuity;
- The more significant volume fraction of carbides did not improve the wear resistance of hardfacing under sliding conditions applied in this study.

5. Acknowledgments

This work was supported by FAPESC (n° 2021TR001820 and n° 2021TR001807), IFSC, and CCMC-UTFPR.

6. References

1. Pradeep GRC, Ramesh A, Durga Prasad B. A review paper on hardfacing processes and materials. *Int J Eng Sci Technol.* 2010;2:6507-10.
2. Bahoosh M, Shahverdi HR, Farnia A. Abrasive wear behavior and its relation with the macro-indentation fracture toughness of an Fe-based super-hard hardfacing deposit. *Tribol Lett.* 2019;67:1-14. <http://dx.doi.org/10.1007/s11249-019-1213-4>.
3. Pawar S, Jha AK, Mulhpadhyay G. Effect of different carbides on the wear resistance of Fe-based hardfacing alloys. *Int J Refract Met Hard Mater.* 2019;78:288-95. <http://dx.doi.org/10.1016/j.jrmhm.2018.10.014>.
4. Tian H, Wang C, Guo M, Tang Z, Wei S, Xu B. Study of the frictional-wear performance and abrasion resistance mechanism of a high-speed arc-sprayed FeNiCrAl coating. *Surf Coat Tech.* 2019;370:320-30. <http://dx.doi.org/10.1016/j.surfcoat.2019.04.092>.
5. Sousa JMS, Lobato MQ, Garcia DN, Machado PC. Abrasion resistance of Fe-Cr-C coating deposited by FCAW welding process. *Wear.* 2021;476:203688. <http://dx.doi.org/10.1016/j.wear.2021.203688>.
6. Shanmugam R, Murugan N. Effect of gas tungsten arc welding process variables on dilution and bead geometry of stellite 6 hardfaced valve seat rings. *Surf Eng.* 2006;22(5):375-83. <http://dx.doi.org/10.1179/174329406X126726>.
7. Hossein A, Farshid MG, Hamid RS. Characterization of Fe49Cr18Mo7B16C4Nb6 high-entropy hardfacing layers produced by gas tungsten arc welding (GTAW) process. *Surf Coat Tech.* 2018;352:360-9. <http://dx.doi.org/10.1016/j.surfcoat.2018.08.019>.
8. Rajeev GP, Kamaraj M, Srinivasa RB. Comparison of microstructure, dilution and wear behavior of Stellite 21 hardfacing on H13 steel using cold metal transfer and plasma transferred arc welding processes. *Surf Coat Tech.* 2019;375:383-94. <http://dx.doi.org/10.1016/j.surfcoat.2019.07.019>.
9. Kashani H, Sadeghi LM, Amadeh A, Khodaghali M, Ahmadzadeh S. The influence of volumetric dilution on the strain induced $\gamma \rightarrow \epsilon$ martensitic transformation in GTAW processed Co-Cr-Mo alloy. *Mater Sci Eng A.* 2008;478(1-2):38-42. <http://dx.doi.org/10.1016/j.msea.2007.05.061>.
10. Chaidemenopoulos NG, Psyllaki P, Pavlidou E, Vourlias G. Aspects on carbides transformations of Fe-based hardfacing deposits. *Surf Coat Tech.* 2019;357:651-61. <http://dx.doi.org/10.1016/j.surfcoat.2018.10.061>.
11. Gahr KHZ, Scholz WG. Fracture toughness of white cast irons. *JOM.* 1980;32:38-44. <http://dx.doi.org/10.1007/BF03354538>.
12. Pintaude G. Strategies for the development of wear-resistant coatings: a review. *Soldag Insp.* 2021;26:1-9. <http://dx.doi.org/10.1590/0104-9224/SI26.16>.
13. Günther K, Bergmann JP, Suchodoll D. Hot wire-assisted gas metal arc welding of hypereutectic FeCrC hardfacing alloys: microstructure and wear properties. *Surf Coat Technol.* 2018;334:420-8. <http://dx.doi.org/10.1016/j.surfcoat.2017.11.059>.
14. Bewley JG. Plasma-transferred-arc wearfacing. *Tooling & Production.* 1980:54-5.
15. Tomaz IV, Colaço FHG, Sarfraz S, Pimenov DY, Gupta MK, Pintaude G. Investigations on quality characteristics in gas tungsten arc welding process using artificial neural network integrated with genetic algorithm. *Int J Adv Manuf Technol.* 2021;113:3569-83. <https://doi.org/10.1007/s00170-021-06846-5>.
16. Colaço FHG, Pintaude G. Combined effects on Fe-Cr-C hardfacing deposited by new technique FCDW-GTAW. *Materia (Rio J).* 2021;26(4):e13097. <http://dx.doi.org/10.1590/S1517-707620210004.1397>.

17. Colaço FHG, Pintaude G. Wear Regimes of Fe–Cr–C hardfacing alloys in microscale abrasion tests. *Tribol Lett.* 2022;70:47. <http://dx.doi.org/10.1007/s11249-022-01590-7>.
18. So H. Characteristics of wear results tested by pin-on-disc at moderate to high speeds. *Tribol Int.* 1996;29(5):415-23. [http://dx.doi.org/10.1016/0301-679X\(95\)00097-N](http://dx.doi.org/10.1016/0301-679X(95)00097-N).
19. ASTM International. G99-17: Standard Test Method for Wear Testing with a Pin-on-Disk Apparatus. West Conshohocken, USA: ASTM International; 2017. <http://dx.doi.org/10.1520/G0099-17>.
20. Nair RP, Griffin D, Randall NX. The use of the pin-on-disk tribology test method to study three unique industrial applications. *Wear.* 2009;267(5-8):823-7. <http://dx.doi.org/10.1016/j.wear.2009.02.026>.
21. Zappelino BF, Almeida EA, Krelling AP, Costa CE, Fontana LC, Milan JC. Tribological behavior of duplex-coating on vanadis 10 cold work tool steel. *Wear.* 2020;203133:442-3. <http://dx.doi.org/10.1016/j.wear.2019.203133>.
22. Archard JF. Contact and rubbing of flat surfaces. *J Appl Phys.* 1953;24:981-8. <http://dx.doi.org/10.1063/1.1721448>.
23. Castle E, Csanádi T, Grasso S, Dusza J, Reece M. Processing and properties of high-entropy ultra-high temperature carbides. *Sci Rep.* 2018;8(1):8609. <http://dx.doi.org/10.1038/s41598-018-26827-1>.
24. Wang Y. Processing and properties of high entropy carbides. *Adv Appl Ceramics.* 2022;121(2):57-78. <http://dx.doi.org/10.1080/17436753.2021.2014277>.
25. Bedolla-Jacuinde A, Guerra FV, Mejía I, Zuno-Silva J, Rainforth M. Abrasive wear of V–Nb–Ti alloyed high-chromium white irons. *Wear.* 2015;332–333:1006-11. <http://dx.doi.org/10.1016/j.wear.2015.01.049>.
26. Novak P, Vojtech D, Serak J. Wear and corrosion resistance of a plasma-nitrided PM tool steel alloyed with niobium. *Surf Coat Tech.* 2006;200:5229-36. <http://dx.doi.org/10.1016/j.surfcoat.2005.06.023>.
27. Podgornik B, Majdic F, Leskovsek V, Vizintin J. Improving tribological properties of tool steels through combination of deep-cryogenic treatment and plasma nitriding. *Wear.* 2012;288:88-93. <https://doi.org/10.1016/j.wear.2011.04.001>.
28. Huq MZ, Celis JP. Expressing wear rate in sliding contacts based on dissipated energy. *Wear.* 2002;252(5-6):375-83. [http://dx.doi.org/10.1016/S0043-1648\(01\)00867-5](http://dx.doi.org/10.1016/S0043-1648(01)00867-5).
29. Çömez N, Çivi C, Durmus H. Reliability evaluation of hardness test methods of hardfacing coatings with hypoeutectic and hypereutectic microstructures. *Int J Miner Metall Mater.* 2019;26(12):1585-93. <http://dx.doi.org/10.1007/s12613-019-1866-x>.
30. Kuo CW, Fan C, Wu SH, Wu W. Microstructure and wear characteristics of hypoeutectic, eutectic and hypereutectic (Cr, Fe)₂₃C₆ carbides in hardfacing alloys. *Mater Trans.* 2007;48(9):2324-8. <http://dx.doi.org/10.2320/matertrans.MB200716>.
31. Bozzi AC, Mello JDB. Wear resistance and wear mechanisms of WC–12%Co thermal sprayed coatings in three-body abrasion. *Wear.* 1999;233-235:575-87. [http://dx.doi.org/10.1016/S0043-1648\(99\)00206-9](http://dx.doi.org/10.1016/S0043-1648(99)00206-9).
32. Rabinowicz E. The wear coefficient: magnitude, scatter, uses. *J of Lubrication Tech.* 1981;103(2):188-94. <http://dx.doi.org/10.1115/1.3251624>.
33. Jokari-Sheshdeh M, Ali Y, Gallo SC, Lin W, Gates JD. Effect of Cr: fe ratio on the mechanical properties of (Cr, Fe)₇C₃ ternary carbides in abrasion-resistant white cast irons. *J Mater Sci.* 2023;58:7504-21. <http://dx.doi.org/10.1007/s10853-023-08461-z>.